Powder Technology 267 (2014) 126–133

Contents lists available at ScienceDirect

Powder Technology

journal homepage: www.elsevier.com/locate/powtec

Solvothermal synthesis and enhanced visible light photocatalytic activity of novel graphitic carbon nitride–Bi_2MoO_6 heterojunctions

Yanlong Tian [a,b], Fuxing Cheng [a], Xiang Zhang [b], Fei Yan [a], Baocheng Zhou [a], Zhi Chen [c], Jiyang Liu [a], Fengna Xi [a], Xiaoping Dong [a,]*

[a] Department of Chemistry, School of Sciences, Zhejiang Sci-Tech University, 928 Second Avenue, Xiasha Higher Education Zone, Hangzhou, China
[b] Center for Composite Material, Harbin Institute of Technology, Harbin, China
[c] College of Materials Science and Engineering, China Jiliang University, Hangzhou, China

ARTICLE INFO

Article history:
Received 3 April 2014
Received in revised form 19 May 2014
Accepted 9 July 2014
Available online 23 July 2014

Keywords:
C_3N_4
Bi_2MoO_6
Heterojunction
Photocatalytic activity

ABSTRACT

Novel graphitic carbon nitride (C_3N_4)–Bi_2MoO_6 heterojunctions with different contents of Bi_2MoO_6 nanosheets were in situ synthesized by a simple solvothermal method. The resulting C_3N_4–Bi_2MoO_6 heterojunctions possess enhanced absorption within the visible light range compared with pure C_3N_4. Meanwhile, these C_3N_4–Bi_2MoO_6 heterojunctions also exhibit much higher photocatalytic activity for methyl orange (MO) degradation than those of single C_3N_4 and Bi_2MoO_6, as well as Degussa P25. Significantly, the optimum photocatalytic activity of the $0.2C_3N_4$–$0.8Bi_2MoO_6$ heterojunction is 3.56 and 3.45 times faster than those of either individual C_3N_4 or Bi_2MoO_6. Based on the trapping experiment results, we believe that photogenerated holes and superoxide radicals $O_2{\bullet}^-$ play a major role in C_3N_4/Bi_2MoO_6 heterogeneous system under visible light irradiation. What is more, the heterojunction displays excellent stability and reusability. This work provides a promising strategy for constructing more C_3N_4 based heterojunctions.

1. Introduction

In the past four decades, semiconductor photocatalytic technique has received wide attention because it provides a green way to directly convert solar energy into chemical energy [1–3]. As a consequence, numerous semiconductor photocatalytic materials (such as metal oxides, sulfides, and oxynitrides) have been developed and applied in photocatalytic degradation of organic pollutants and photo-induced splitting of water [4–10]. Recently, graphitic carbon nitride (C_3N_4), an analog of graphite, was reported as a novel metal-free photocatalyst for efficient hydrogen generation from water splitting under visible light irradiation [11]. C_3N_4 also exhibited a high visible light photocatalytic performance for the degradation of organic pollutants [12–14]. This material would be a promising photocatalyst owing to its absorption of visible light (2.70 eV), low price, and high stability, along with its unique chemical and catalytic properties [15]. Nevertheless, the photocatalytic performance of pristine C_3N_4 was still relatively moderate due to its low quantum yield originating from high recombination rate of photogenerated electron–hole pairs. Therefore, many attempts have been devoted to further improve the photocatalytic performance of pristine C_3N_4, for instance, doping with metal or nonmetal elements, introduction of nano-/mesoporous structure, coupling with graphene, *etc.* [16–21].

It is well-known that the construction of heterojunction by coupling of two different semiconductors with matched band potentials is a feasible approach for enhancing quantum yield of semiconductor [22–24]. In such heterogeneous system, photogenerated electrons and holes could effectively separate through a charge transfer between two coupling semiconductors, thereby reducing their recombination. Not surprisingly, this strategy was also employed for improving the photocatalytic activity of C_3N_4 once this material was introduced into photocatalysis. Several kinds of C_3N_4 based heterojunctions have been obtained, including C_3N_4–WO_3, C_3N_4–BiOBr, C_3N_4–BiOCl, C_3N_4–CdS, C_3N_4–Bi_2WO_6, C_3N_4–$ZnWO_4$, and C_3N_4–$BiVO_4$ [25–33]. These C_3N_4 based heterojunctions, without exception, exhibited enhanced photocatalytic activities compared with individual C_3N_4.

Bismuth molybdate (Bi_2MoO_6), a Ternary bismuth oxide compound with Aurinillius structure, owns a unique layered structure sandwiched between the perovskite octahedral $(MoO_4)^{2-}$ sheets and the $(Bi_2O_2)^{2+}$ layers [34]. Such a layered structure is beneficial to charge transfer, and thereby could reduce the recombination of photogenerated carriers. Additionally, the band gap of Bi_2MoO_6 is quite narrow and only 2.60 eV [35]. These excellent structural and spectral properties make Bi_2MoO_6 exhibit excellent visible light photocatalytic activities [34–37]. Most recently, Bi_2MoO_6 was also used as a fundamental component to construct semiconductor heterojunction with high visible light activities [38–40]. Motivated by these works, we investigated the band positions of C_3N_4 and Bi_2MoO_6 and fortunately found that both the conduction band (CB) bottom and valence band (VB) top of C_3N_4

---

* Corresponding author. Tel.: +86 571 86843228; fax: +86 571 86843653.
E-mail address: xpdong@zstu.edu.cn (X. Dong).

http://dx.doi.org/10.1016/j.powtec.2014.07.021

are higher than those of Bi_2MoO_6. This result implies that it is possible to form C_3N_4–Bi_2MoO_6 heterojunction by coupling C_3N_4 and Bi_2MoO_6.

Herein, we fabricated a novel C_3N_4–Bi_2MoO_6 heterojunction by a solvothermal method for the first time. The photocatalytic performance of C_3N_4–Bi_2MoO_6 heterojunction was evaluated by degrading MO under visible light irradiation. We also used a variety of characterization techniques to study the crystal structure, morphology, and optical property of C_3N_4–Bi_2MoO_6 heterojunction. What is more, a possible photocatalytic mechanism of this heterojunction was also discussed based on the experimental result in detail.

2. Experimental section

2.1. Preparation of C_3N_4

All reagents used in this study were of analytical purity without further purification. The pure C_3N_4 was prepared by thermal polycondensation of melamine following our previously reported method [26]. In detail, 10 g of melamine was put into a semiclosed alumina crucible with a cover and heated at 520 °C for 4 h in a muffle furnace with a ramping rate of 10 °C min^{-1}. The obtained yellow solid was ground into a powder for further use.

2.2. Fabrication of C_3N_4–Bi_2MoO_6 heterojunctions

A typical synthetic procedure of C_3N_4–Bi_2MoO_6 heterojunctions was as follows: a desired amount of $Na_2MoO_6 \cdot 2H_2O$ was dissolved in a mixed solution of ethylene glycol (10 mL) and ethanol (60 mL) to form a clear solution. Subsequently, an appropriate amount of C_3N_4 powder was homogeneously dispersed in this clear solution *via* 5 min of sonication, and then a solution of ethylene glycol (10 mL) containing a stoichiometric amount of $Bi(NO_3)_3 \cdot 5H_2O$ was quickly added. After vigorously stirring for 30 min, the suspension was transferred to an autoclave with an inner Teflon lining and maintained at 160 °C for 24 h. Finally, the precipitate was collected, washed several times with deionized water and ethanol, dried at 60 °C for 12 h, and milled for further use. According to this method, we have obtained different mass ratios of C_3N_4–Bi_2MoO_6 heterojunctions at 4:6, 3:7, 2:8, and 1:9 by tuning the precursor concentration for synthesizing Bi_2MoO_6, and named as $0.4C_3N_4$–$0.6Bi_2MoO_6$, $0.3C_3N_4$–$0.7Bi_2MoO_6$, $0.2C_3N_4$–$0.8Bi_2MoO_6$, $0.1C_3N_4$–$0.9Bi_2MoO_6$, respectively. For comparison, the pure Bi_2MoO_6 sample was also prepared under the same conditions without the addition of C_3N_4 powder.

In addition, we have also synthesized some other materials as reference photocatalysts, including N-modified TiO_2, mechanically mixed $0.2C_3N_4$–$0.8Bi_2MoO_6$, $0.2C_3N_4$–$0.8TiO_2$, and $0.2TiO_2$–$0.8Bi_2MoO_6$, to use in photocatalytic tests. The details of the synthesis of these reference photocatalysts were all listed in the Supporting information.

2.3. Characterization

X-ray diffraction (XRD) patterns were characterized on a DX-2700 diffractometer (Dandong Haoyuan Instrument Co. Ltd., China) using Cu Kα radiation ($\lambda = 0.15418$ nm). Scanning electron microscopy (SEM) images and energy dispersive X-ray spectroscopy (EDS) maps were observed with a Hitachi S-4800 Field emission scanning electron microscope. Transmission electron microscopy (TEM) observation was obtained on a JEOL JEM-2100 electron microscope with an accelerating voltage of 200 kV. Fourier transform infrared (FT-IR) spectra were recorded on a Nicolet Avatar 370 spectrophotometer using the standard KBr disk method. Diffuse reflectance spectra were taken on a Shimadzu 2450 UV–vis spectrometer with an integrating sphere using $BaSO_4$ as the reference. Photoluminescence (PL) spectra of the samples were measured using a Shimadzu RF5301PC fluorescence spectrophotometer.

2.4. Photocatalytic tests

The photocatalytic tests were performed in a 150 mL of quartz glass reactor, which was cooled by recycled water to prevent the thermal catalytic effect. A 300 W xenon lamp (HSX-F300, Beijing NBet) with a 420 nm cutoff filter was used as a visible light source to trigger the photocatalytic reaction. MO and 2,4-dichlorophenol (2,4-DCP) were selected as probe dyes to evaluate the photocatalytic activities of as-synthesized photocatalysts. In each experiment, 100 mg of photocatalyst was added into 100 mL aqueous solution of MO (5 mg L^{-1}) or 2,4-DCP (20 mg L^{-1}), and the distance between cutoff filter and the surface of the solution was set at 15 cm. Before illumination, the suspension was stirred in the dark for 1 h to establish adsorption–desorption equilibrium between photocatalyst and dye molecules. At given irradiation time intervals, 3 mL of the suspension was sampled and subsequently centrifuged to remove the photocatalyst powders. The concentration was monitored by measuring the maximum absorbance at 463 nm for MO and 283 nm for 2,4-DCP through a Shimadzu UV-2450 spectrophotometer.

3. Results and discussions

3.1. Structure, morphology and composition of C_3N_4–Bi_2MoO_6 heterojunctions

The XRD patterns of C_3N_4, Bi_2MoO_6, and C_3N_4–Bi_2MoO_6 heterojunctions are shown in Fig. 1. The XRD diffraction peaks of the pure Bi_2MoO_6 appear at 10.89°, 23.55°, 28.21°, 32.52°, 36.01°, 46.78°, 55.45°, and 58.43°, which match well with the (020), (111), (131), (200), (151), (202), (331), and (262) crystal planes of orthorhombic Bi_2MoO_6 (JCPDS 76-2388). After coupling with C_3N_4, all these diffraction peaks are still present in the XRD patterns of C_3N_4–Bi_2MoO_6 heterojunctions, clearly suggesting that the heterogeneous process would not give rise to any influence on the crystal structure of Bi_2MoO_6. The pure C_3N_4 displays two pronounced peaks of 13.04° and 27.47°, which are perfectly indexed to the (100) and (002) crystal planes of graphite-like carbon nitride (JCPDS 87-1526), corresponding to the characteristic in-plane structural packing motif of tristriazine units and interlayer stacking of conjugated aromatic system, respectively [11]. However, these two diffraction peaks cannot be found in heterojunctions, this is mainly because C_3N_4 layer was too thin [31, 32]. Similar results are also observed in some other C_3N_4 based heterojunctions, such as C_3N_4–$ZnWO_4$ and C_3N_4–Bi_2WO_6 [30–32].

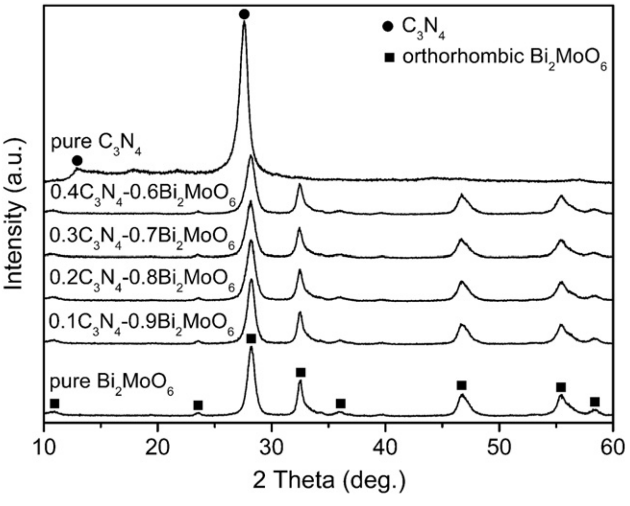

Fig. 1. XRD patterns of C_3N_4, Bi_2MoO_6, and C_3N_4–Bi_2MoO_6 heterojunctions.